iScience

CellPress
OPEN ACCESS

Article

Mechanistic insights into CDCP1 clustering on non-small-cell lung cancer membranes revealed by super-resolution fluorescent imaging

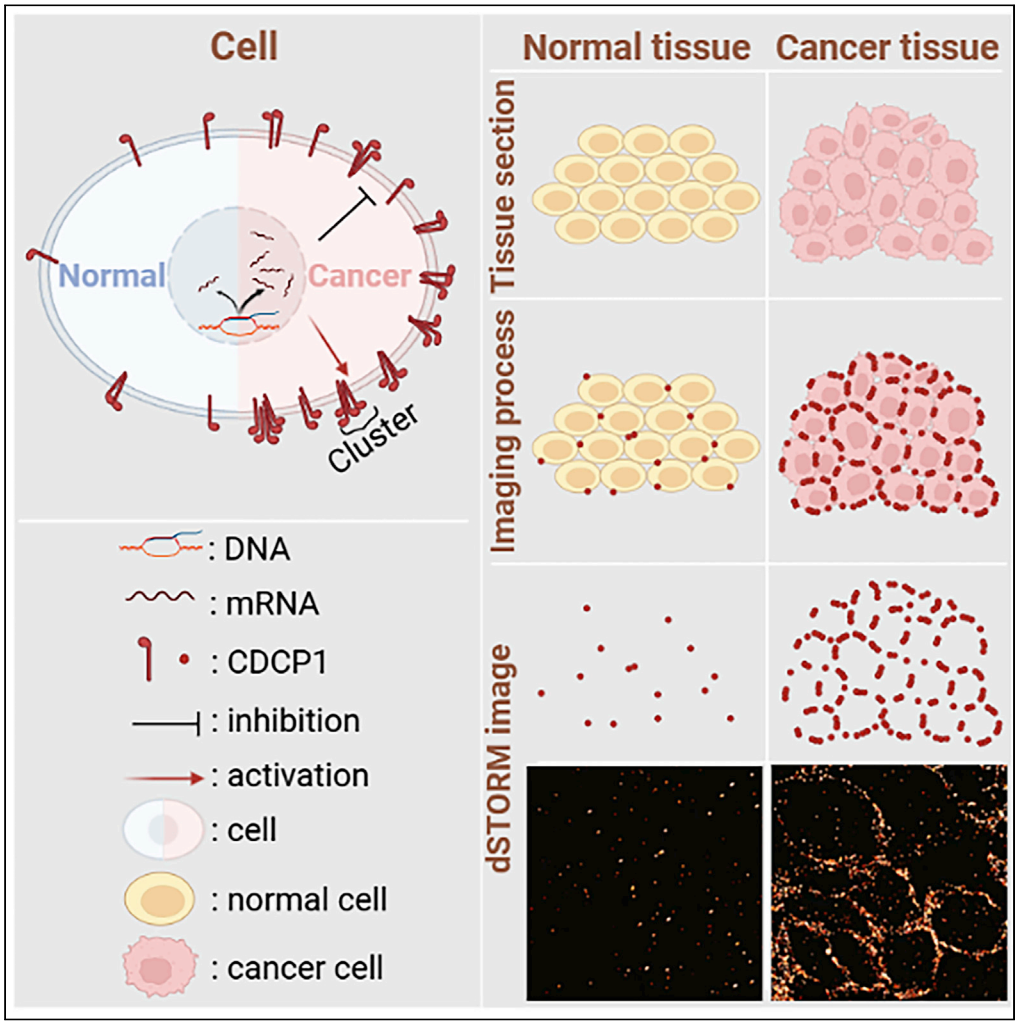

Xiao Qi, Zihao Li, Jinrui Zhang, ..., Hongda Wang, Ti Tong, Jing Gao

tongti@jlu.edu.cn (T.T.)
gaojing@ciac.ac.cn (J.G.)

Highlights

dSTORM imaging reveals the nanoscale clustering distribution of CDCP1 on cell membrane

CDCP1 forms larger and denser clusters on lung cancer cells than normal cells

The clustered distribution of CDCP1 on cancer cells is affected by its activity

dSTORM imaging of tissue reflects CDCP1 distribution in tumor microenvironment

Qi et al., iScience 26, 106103
March 17, 2023
https://doi.org/10.1016/j.isci.2023.106103

iScience

CellPress
OPEN ACCESS

Article

Mechanistic insights into CDCP1 clustering on non-small-cell lung cancer membranes revealed by super-resolution fluorescent imaging

Xiao Qi,[1] Zihao Li,[1] Jinrui Zhang,[2] Hongru Li,[2,3] Guangxin Zhang,[1] Meng Li,[1] Baofeng Li,[1] Yilin Fu,[4] Mingjun Cai,[2] Hongda Wang,[2,3,5] Ti Tong,[1,6,*] and Jing Gao[2,*]

SUMMARY

CDCP1 is a transmembrane protein that is involved in a variety of important biological processes and upregulated in a variety of human solid malignancies; however, its spatial distribution and variation at the molecular level remain unclear. To solve this problem, we first analyzed its expression level and prognostic implications in lung cancer. Then, we used super-resolution microscopy to reveal the spatial organization of CDCP1 at different levels, and found that cancer cells generated more and larger CDCP1 clusters than normal cells. Furthermore, we found that CDCP1 can be integrated into larger and denser clusters as functional domains upon activation. Our findings elucidated the significant differences of CDCP1 clustering characteristics between cancer and normal cells, and revealed the relationship between its distribution and function, which will contribute to a comprehensive understanding of its oncogenic mechanism, and will be of great help for the development of CDCP1-targeted drugs for lung cancer.

INTRODUCTION

Lung cancer is one of the most common cancer and the main cause of cancer-related death.[1] According to pathological types, it can be divided into small-cell lung cancer and non-small-cell lung cancer (NSCLC), the latter of which accounts for about 85%.[2] The 5-year survival rate for NSCLC is still lower than that for many other cancers, despite progress in video-assisted thoracoscopic surgery and medical therapies.[1–3] Luckily, the advancement of targeted therapy and biomarker detection has benefited a large number of patients.[3] Thus, it is essential to find a suitable biomarker and therapeutic target to improve the prognosis of NSCLC.

CDCP1, a single-channel transmembrane protein,[4] is overexpressed in NSCLC and is significantly associated with poor prognosis in patients.[5–8] In malignant tumor cells, CDCP1 can be activated by Src kinase, which promotes the proliferation, invasion, and metastasis of tumor cells through classic signaling pathways such as MAPK (Ras/ERK) and PI3K/AKT.[9–13] Besides, numerous studies have demonstrated that antibodies targeting CDCP1, including MAB41-2, MAB10-D7, and C20Fc, can inhibit tumor growth and metastasis in various animal models and improve the efficacy of chemotherapy drugs.[3,14–17] Hence, its overexpression on cancer cells and crucial roles in tumor progression make CDCP1 a potential target for diagnosis and treatment.

Previous research studies on CDCP1 have been carried out mainly by Western blot, confocal microscopy, immunohistochemistry, and other methods to reflect the overall level.[6,18] However, the differences of its spatial distribution between cancer cells and normal cells and the relationship between its distribution and function are still unclear. In addition, there are few studies on super-resolution imaging of tissue sections, so the distribution of CDCP1 molecules in tissues has not been fully characterized. Here, we first analyzed the expression level of CDCP1 in pan-cancer and its correlation with lung cancer prognosis using Gepia2 and Kaplan-Meier plotter databases. Then, we used the super-resolution imaging technique, direct stochastic optical reconstruction microscopy (dSTORM), which can break the optical diffraction limit and provide super-resolution imaging with tens of nanometers,[19,20] to reveal the distribution differences of CDCP1 between cancer cells and normal cells. We observed its spatial organization on cell membrane from cellular level to tissue level. It was found that the expression level of CDCP1 was significantly increased

[1]Department of Thoracic Surgery, the Second Hospital of Jilin University, Changchun, Jilin 130041, China

[2]State Key Laboratory of Electroanalytical Chemistry, Research Center of Biomembranomics, Changchun Institute of Applied Chemistry, Chinese Academy of Sciences, Changchun, Jilin 130022, China

[3]University of Science and Technology of China, Hefei, Anhui 230027, China

[4]Department of Thoracic Surgery, Shandong Provincial Hospital Affiliated to Shandong First Medical University, Jinan, Shandong 250021, China

[5]Laboratory for Marine Biology and Biotechnology, Qing dao National Laboratory for Marine Science and Technology, Wenhai Road, Aoshanwei, Jimo, Qingdao, Shandong 266237, China

[6]Lead contact

*Correspondence: tongti@jlu.edu.cn (T.T.), gaojing@ciac.ac.cn (J.G.)

https://doi.org/10.1016/j.isci.2023.106103

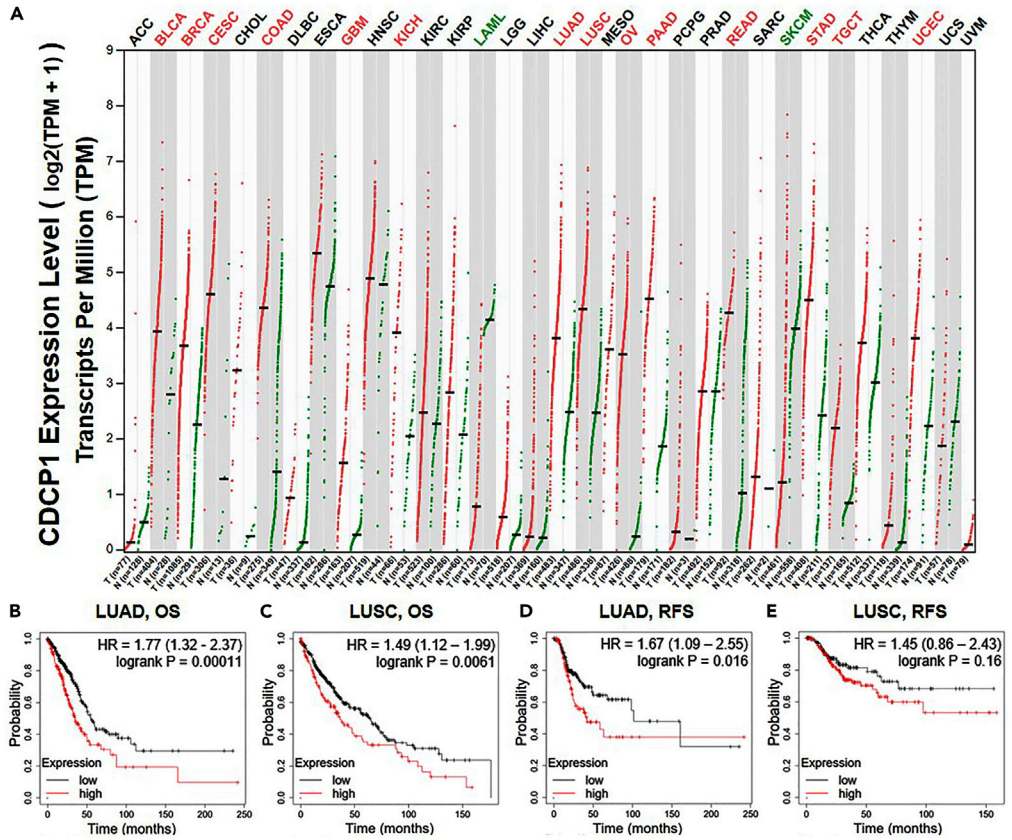

Figure 1. The level of CDCP1 mRNA in pan-cancer and its prognostic significance in NSCLC

(A) The mRNA level of CDCP1 in different types of human cancer (Gepia2). In the name of cancer type, red represents a significantly higher expression level and green represents a significantly lower expression level. T for tumor tissue and N for normal tissue.

(B–D) Kaplan-Meier survival curve analysis of the prognostic value of high and low expression of CDCP1 in patients with LUAD and LUSC (Kaplan-Meier plotter). High CDCP1 expression was associated with worse OS (B) and RFS (D) in LUAD. High CDCP1 expression was associated with worse OS in LUSC (C). Survival curves of RFS in LUSC (E). LUAD, lung adenocarcinoma; LUSC, lung squamous cell carcinoma; OS, overall survival; RFS, recurrence-free survival.

and it tended to aggregate into clusters on the membrane of cancer cells. These differences were particularly significant in tissues. Furthermore, we explored the relationship between its distribution and function by regulating its activity with EGF (promotion) or PP2 (inhibition) reagents, respectively.

Together, our work reveals the distribution pattern of CDCP1 from mRNA to protein, from cell to tissue at the single molecule level, and associated its spatial organization with its activation, which will contribute to a comprehensive understanding of its oncogenic mechanism, and will be of great help for the development of CDCP1-targeted biomarkers and drugs for lung cancer.

RESULTS AND DISCUSSION

The level of CDCP1 mRNA and its prognostic significance in NSCLC

Gene expression analyses by the Gepia2 database showed that CDCP1 mRNA levels were dramatically higher in most malignant tumors compared with the corresponding normal tissues, such as bladder, breast, lung, and other cancer types (Figure 1A). The full names of all tumor abbreviations were shown in Table S1. For lung cancer, CDCP1 expression in NSCLC including lung adenocarcinoma (LUAD) and lung squamous cell carcinoma (LUSC) was significantly higher than that in normal lung tissues. Then, the prognostic value of CDCP1 expression in human lung cancers was analyzed by the Kaplan-Meier plotter database. In LUAD, higher expression of CDCP1 was significantly associated with poorer overall survival (OS) and recurrence-free survival (RFS) (Figures 1B and 1D). Besides, the overexpression of CDCP1 was significantly associated

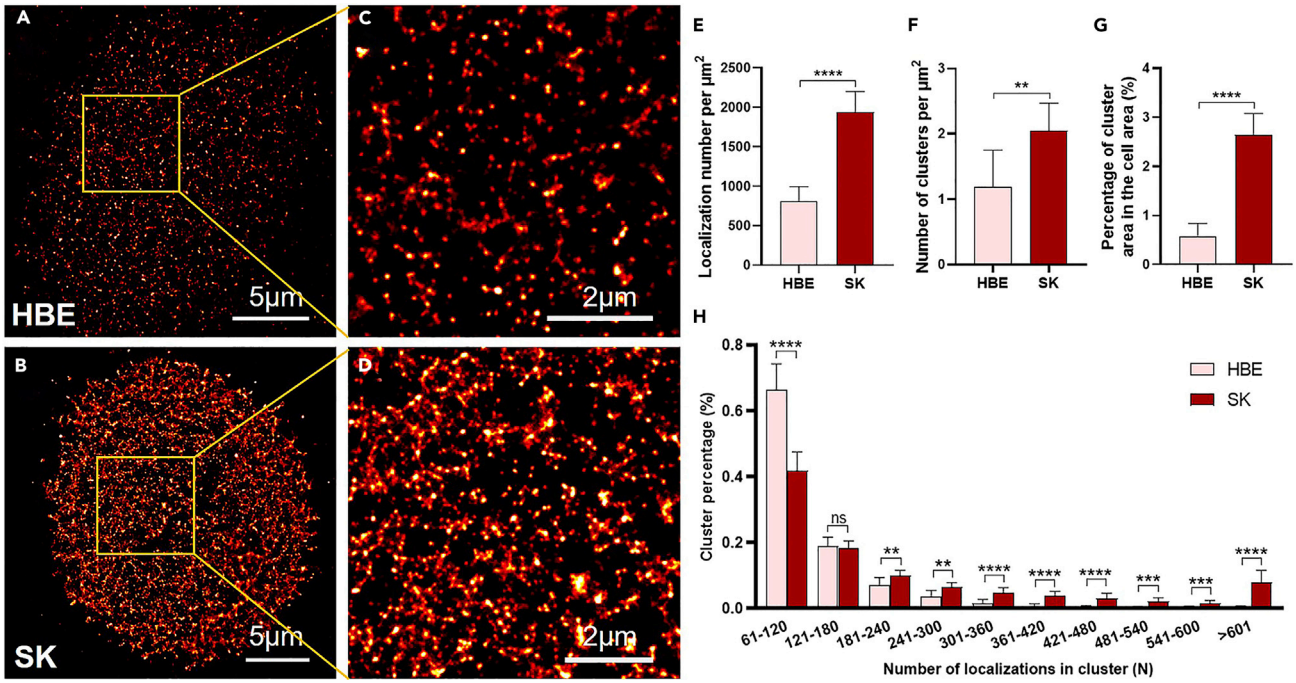

Figure 2. CDCP1 proteins formed different numbers and sizes of clusters on cultured lung cancer cells and normal cells

(A and B) Reconstructed dSTORM images of CDCP1 on HBE cell (A) and SK-MES-1 cell membrane (B).

(C and D) The corresponding magnified images of (A and B). (Scale bars: a and b, 5 μm; c and d, 2 μm).

(E) The number of CDCP1 localizations per μm^2 on HBE and SK-MES-1 cell membranes.

(F) The number of CDCP1 clusters per μm^2.

(G) The percentage of CDCP1 cluster area in each cell.

(H) The percentage of CDCP1 clusters containing different number of localizations. All data were obtained from 10 cell samples in 3 independent experiments (mean ± SD) and statistical significance was processed by two-tailed unpaired t-test. **p < 0.01, ***p < 0.001, ****p < 0.0001, and ns means not significant.

with poor OS in LUSC while it was not associated with RFS in LUSC (Figures 1C and 1E). These results proved that CDCP1 was overexpressed in a variety of cancer tissues, including lung cancer, and also demonstrated the prognostic significance of CDCP1 expression in LUAD and AUSC. Since CDCP1 mRNA level was significantly increased in lung cancer and was associated with poor prognosis, it is expected to become a new target for lung cancer diagnosis and treatment.

Super-resolution imaging of CDCP1 on cultured and primary lung cells

To further explore the protein expression and the distribution at single molecule level, we first used dSTORM to observe CDCP1 on the cancer cell (SK-MES-1) and the normal cell (HBE) membranes. The reconstructed dSTORM images showed that CDCP1 was less expressed on HBE cell surfaces than SK-MES-1 cell surfaces (Figures 2A and 2B). The corresponding enlarged images showed that CDCP1 formed larger and more clusters on cancer cells, while it tended to be scattered on normal cells (Figures 2C and 2D). Statistical data indicated that the localization density of CDCP1 on cancer cells was about twice that on normal cells (1943 ± 260 vs. 807 ± 188 per μm2) (Figure 2E).

To further analyze the clustering features of CDCP1, we used SR-Tesseler,[21] a graphic processing method based on Voronoï diagram, to segment and quantify the super-resolution imaging data[22] (see the data analysis for details). Before using the software, we measured the parameters of the fluorescent secondary antibody which were diluted 1,000 times, and calculated that the localization number of single fluorophores was about 61 (See Figures S1A and S1B), which was taken as the minimum value of the localization number in one cluster. The results showed that the number of CDCP1 clusters per μm^2 on cancer cells was significantly higher than that on normal cells (SK-MES-1: 2.05 ± 0.42 per μm^2, HBE: 1.19 ± 0.56 per μm^2) (Figure 2F). The percentage of cluster area in cancer cells was significantly greater than that in normal cells (SK-MES-1: 2.65 ± 0.43%, HBE: 0.58 ± 0.26%) (Figure 2G).

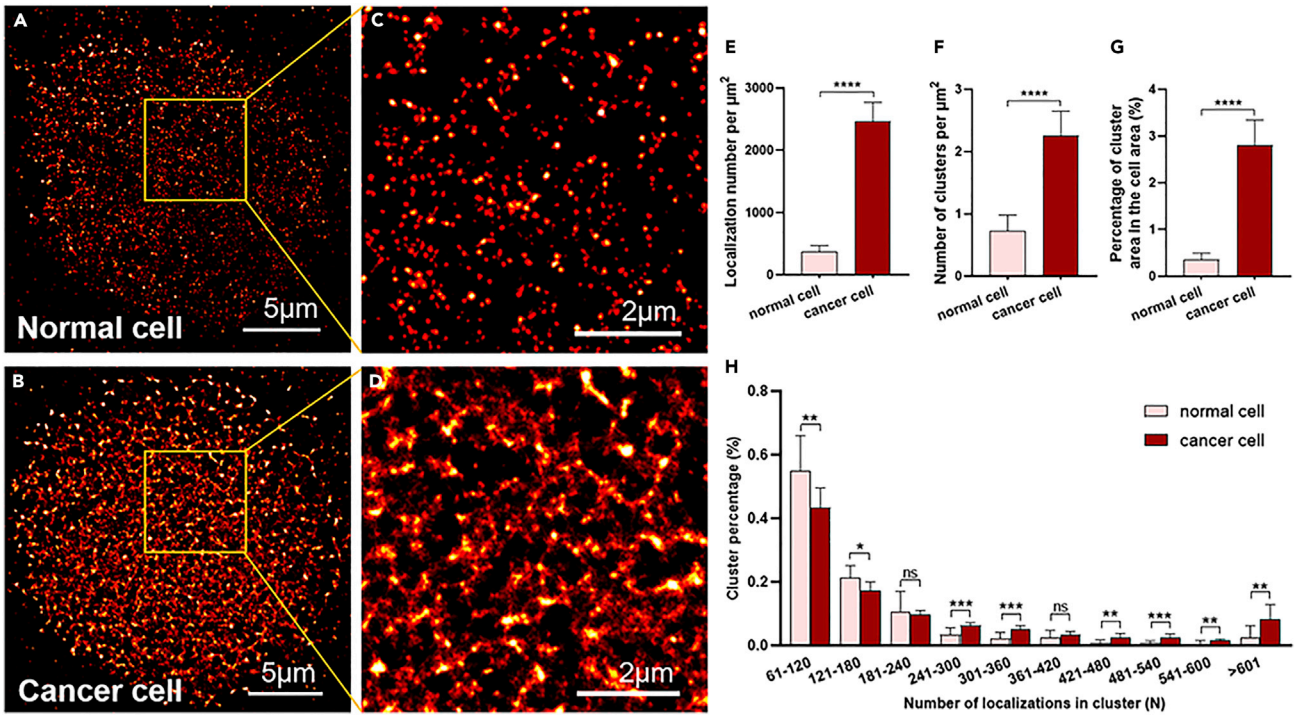

Figure 3. The distribution of CDCP1 on primary non-small lung cancer cells and normal cells

(A and B) Reconstructed dSTORM images of CDCP1 on primary normal cell (A) and primary non-small lung cancer cell membrane (B).

(C and D) The corresponding magnified images of (A and B). (Scale bars: A and B, 5 μm; C and D, 2 μm).

(E) The number of CDCP1 localizations per μm^2 on primary non-small lung cancer cell and normal cell membranes.

(F) The number of CDCP1 clusters per μm^2.

(G) The percentage of CDCP1 cluster area in each cell.

(H) The percentage of CDCP1 clusters containing different number of localizations. All data were obtained from 10 cell samples in 3 independent experiments (mean ± SD) and statistical significance was processed by two-tailed unpaired t-test. *p < 0.05, **p < 0.01, ***p < 0.001, ****p < 0.0001, and ns means not significant.

Moreover, the small clusters (localizations <120) on normal cells accounted for more than 60% and almost 95% of clusters contained less than 300 localizations, while the cancer cells had more dense clusters (localizations >181) than normal cells (Figure 2H). We also analyzed the expression of CDCP1 in these two cell lines by Western Blot, and the results showed that CDCP1 protein level in SK-MES-1 cells was significantly higher than that in HBE cells (Figures 7I and 7J).

To verify the clustered distribution of CDCP1 in lung cancer, we then isolated NSCLC cells and the paired normal lung epithelial cells from patients to observe. The reconstructed dSTORM images also showed that CDCP1 was overexpressed in primary lung cancer cells than that in normal lung cells (Figures 3A and 3B). In the corresponding magnification image, there were more and larger protein clusters on lung cancer cell membranes, while normal lung cells had fewer and smaller clusters (Figures 3C and 3D). Statistical data indicated that the localization density in primary lung cancer cells was nearly 6 times higher than that in normal lung cells (2468 ± 303 vs. 377 ± 95 per μm^2) (Figure 3E). SR-Tesseler analysis demonstrated that the number of clusters (2.26 ± 0.40 vs. 0.72 ± 0.26 per μm^2) and the proportion of cluster area (2.8 ± 0.54% vs. 0.36 ± 0.14%) in cancer cells were both significantly higher than those on normal cells (Figures 3F and 3G). We also found that there were more denser clusters with localizations between 241 and 360 and localizations more than 421 on cancer cells, while in normal cells, there were almost smaller clusters that contained no more than 180 localizations (Figure 3H). These results were consistent with those obtained from cultured cell lines, further confirming the overexpression and clustering of CDCP1 in lung cancer.

The data above indicated that CDCP1 proteins were highly expressed in lung cancer cells, and formed larger and denser clusters than those in normal cells. Especially in extracted primary cells, the

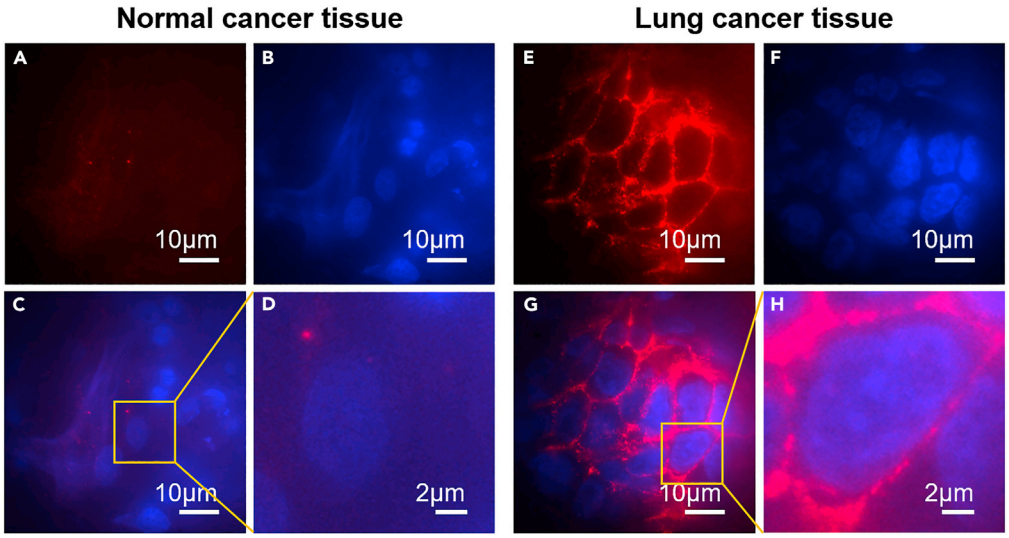

Figure 4. Imaging of cancer tissue and matched normal tissue sections under the common fluorescent microscope (100×)

(A and E) Images of immunofluorescent staining of CDCP1 protein in fluorescent-field illumination.

(B and F) Nuclear staining images.

(C and G) The merged images of CDCP1 protein and nucleus.

(D and H) The corresponding magnified images of (C and G). (Scale bars: A–C and E–G, 10 μm; D and H, 2 μm).

differences of expression and distribution were more obvious. A growing number of studies have shown that CDCP1 can bind itself or other cancer-related membrane proteins such as EGFR and HER2 to form dimers, which promote metastasis and treatment resistance in cancer cells.[23,24] Therefore, we speculated that CDCP1 clusters on the lung cancer cell membranes are functional units which facilitate development of cancer and signal transduction. On the contrary, there were a few CDCP1 clusters in normal cells, which can explain why CDCP1 was expressed but did not function as a cancer-related protein in normal cells.[25]

Clusters of CDCP1 on primary lung cancer tissues

To further visualize the distribution of CDCP1 protein on cancer cell membranes in the tumor microenvironment, we *in situ* imaged pathological tissues including lung cancer tissue sections and the adjacent normal tissue sections from the same patient. First, we used a common fluorescent microscope (100 x) to observe the cancer tissue and the matched normal tissue, and found that CDCP1 was mainly distributed on the cell membrane and overexpressed in cancer cells (Figures 4A–4C, e-g). However, in the enlarged images of the corresponding individual cell, we can only get the blurred outline of CDCP1 distribution on the membrane (Figures 4D and 4H).

Therefore, we next used super-resolution fluorescent microscopy (100 x) for imaging. Figures 5A and 5G showed the images of tissue sections under bright-field illumination, and the corresponding TIRF images were shown in Figures 5B and 5H, respectively. We found that CDCP1 was low expression and sparsely distributed in normal tissues, but overexpression and densely distributed in lung cancer tissues (Figures 5C and 5I). The statistical analysis showed that there was a high density of localization on cancer tissues (cancer tissue: 567 $\pm$ 99 per μm^2, normal tissue: 34 $\pm$ 31 per μm^2) (Figure 5M). In the corresponding magnified image, we could clearly observe that CDCP1 was unevenly distributed on the cell membrane and formed different sizes of clusters (Figures 5D and 5J). We used SR-Tesseler to quantitatively analyze them, and found that the protein clusters in cancer tissues were more numerous and larger than those in normal tissues (Figures 5E, 5F, 5K, and 5L).

Statistical analysis showed that the area of protein clusters in cancer tissue accounted for about 1.71 $\pm$ 0.51% of the cell membrane area, and the number of clusters per μm^2 was about 1.04 $\pm$ 0.22; while in normal tissues, there were almost no clusters (number of clusters per μm^2: 0.05 $\pm$ 0.05; percentage of

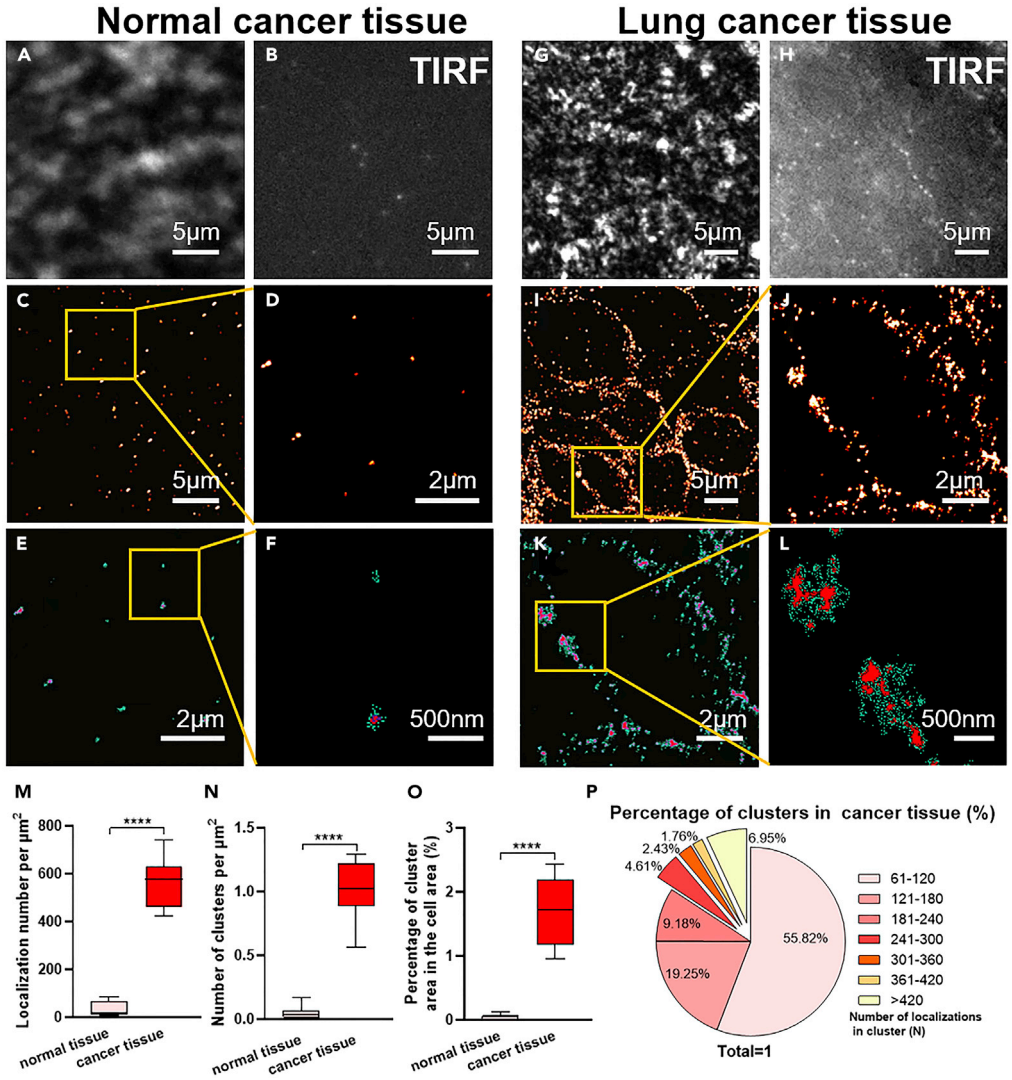

Figure 5. The super-resolution images of cancer tissue and matched normal tissue sections (100×)

(A and G) Images of cancer tissue and normal tissue sections in bright-field illumination.

(B and H) TIRF images of CDCP1 on normal tissue section (B) and cancer tissue section (H).

(C and I) Reconstructed dSTORM images of CDCP1 on cancer tissue and matched normal tissue sections, and (D and J) the corresponding magnified images.

(E and K) The corresponding cluster distribution images of (D and J) analyzed by SR-Tesseler (red areas represent clusters).

(F and L) The progressively zoomed regions of (E and K). (Scale bars: A–C and G–I, 5 μm; D, E and J, K, 2 μm; F and L, 500 nm).

(M) The number of CDCP1 localizations per μm^2 on cancer tissue and matched normal tissue sections.

(N) The number of CDCP1 clusters per μm^2.

(O) The percentage of CDCP1 cluster area in each cell.

(P) The percentage of CDCP1 clusters containing different number of localizations in cancer tissues. All data were obtained from 10 cell samples in 3 independent experiments (mean ± SD) and statistical significance was processed by two-tailed unpaired t-test. ****$p < 0.0001$.

cluster area in the cell area: 0.05 ± 0.04%) (Figures 5N and 5O). Moreover, there was about 16% of the clusters containing more than 241 localizations (Figure 5P) in cancer tissues. This pattern of distribution was similar to that in cells.

Together, we used the super-resolution fluorescent microscope to observe the precise localization of proteins in tissues that could not be seen by common fluorescent microscope. Due to the affection of

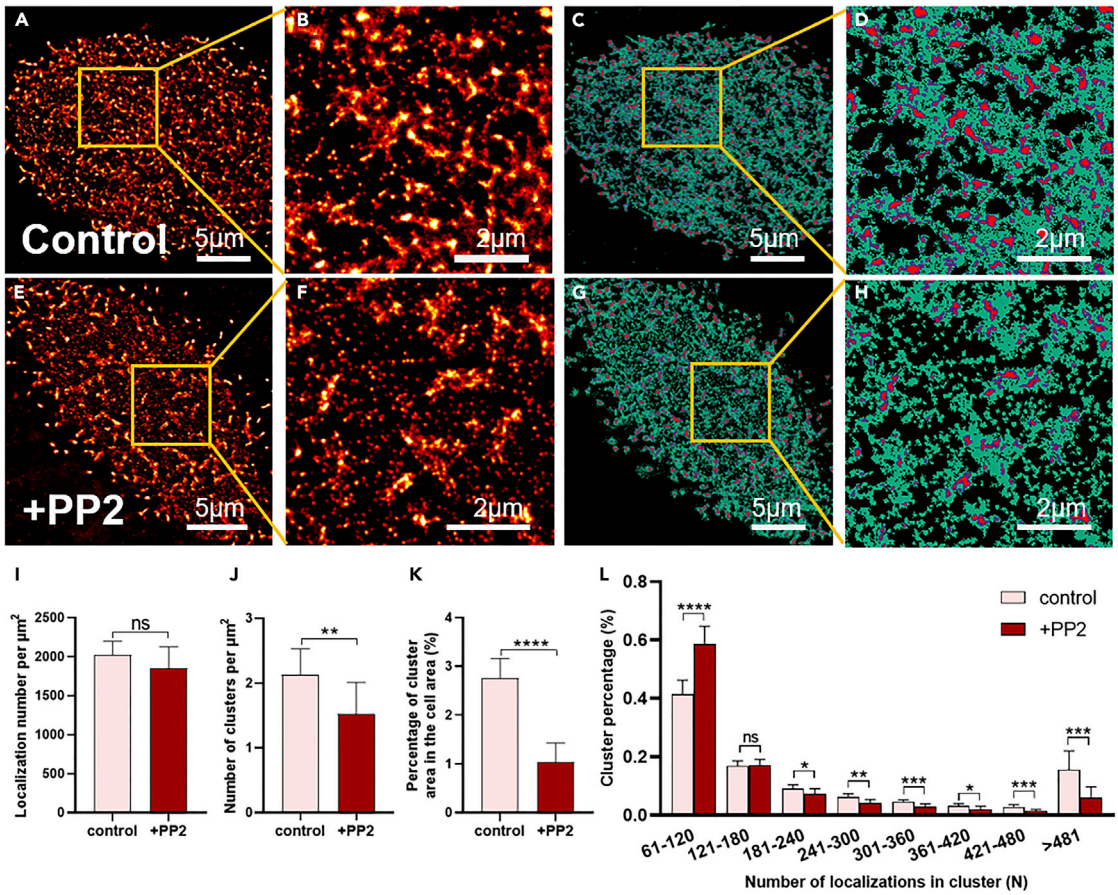

Figure 6. The changes of CDCP1 clusters after treatment of PP2

(A, B, E, and F) Reconstructed dSTORM images of CDCP1 on control (A) and PP2-treated (E) SK-MES-1 cell membranes, and the corresponding magnified images (B and F).

(C, D, G, and H) The corresponding cluster distribution images of (A, B, E, and F) analyzed by SR-Tesseler (red areas represent clusters). (Scale bars: 5 μm for A, E, C, G; 2 μm for B, F, D, H.).

(I) The number of CDCP1 localizations per μm^2 on control and PP2-treated SK-MES-1 cell membranes.

(J) The number of CDCP1 clusters per μm^2.

(K) The percentage of CDCP1 cluster area in each cell.

(L) The percentage of CDCP1 clusters containing different number of localizations. All data were obtained from 10 cell samples in 3 independent experiments (mean ± SD) and statistical significance was processed by two-tailed unpaired t-test. *$p < 0.05$, **$p < 0.01$, ***$p < 0.001$, ****$p < 0.0001$, and ns means not significant.

complex tumor microenvironment in patients, the distribution of CDCP1 in tissues was influenced by the combination of cell self-regulation, cell-cell interaction, and stimulation of various signaling molecule in the extracellular environment. From primary cells to tissue imaging, we both observed the feature of protein clustering, which demonstrated the authenticity of the conclusion and the reliability of *in situ* observation of tissue sections. Besides, CDCP1 was overexpressed, densely distributed, and formed different sizes of clusters in NSCLC, which may be related to the role of CDCP1 in promoting tumorigenesis and progression.

Src kinase inhibitors attenuate the aggregation of CDCP1 in cancer cells

The intracellular domain of CDCP1 has multiple tyrosine residues that can be phosphorylated by Src kinase family, and the activated CDCP1 promotes migration and invasion of malignant tumor cells.[26–28] For tumor cells, inhibition of CDCP1 activity or reduction of CDCP1 expression level can limit anchorage-independent survival which plays a vital role in tumor metastasis.[29,30] Based on the experiments above, we hypothesized that CDCP1 protein clusters may be functional domains that promote proliferation and

metastasis of cancer cells. To explore the relationship between the distribution of CDCP1 and its activation status, we inhibited its activity with PP2 (Src kinase inhibitor) and then observed whether its distribution was affected.

As shown in the dSTORM images (Figures 6A, 6B, 6E, and 6F), we found that the aggregation of CDCP1 on the cell surface was significantly reduced after treated with 2 μM PP2 for 24 h. Although, data analysis showed that inhibitor did not change the localization density of CDCP1 molecules (control: 2024 ± 171 per μm^2, +PP2: 1853 ± 272 per μm^2) (Figure 6I). Further analysis by SR-Tesseler, however, showed that PP2 significantly reduced the degree of its aggregation (Figures 6C, 6D, 6G, and 6H). And the number of clusters decreased significantly from 2.13 ± 0.40 to 1.52 ± 0.49 per μm^2 (Figure 6J). Moreover, the percentage of cluster area in SK-MES-1 cells treated with PP2 decreased to more than half of that in the untreated cells (control: 2.76 ± 0.40%, +PP2: 1.03 ± 0.40%) (Figure 6K). As for CDCP1 cluster size, the percentage of small clusters that contained no more than 120 localizations increased and that of large clusters with localizations more than 181 decreased significantly (Figure 6L).

These findings demonstrated that PP2 decreased the clustering level of CDCP1 and caused large clusters to become small clusters or even sparse distribution, although the localization density of CDCP1 was unchanged. The inhibition of CDCP1 mainly altered the degree of its aggregation, especially the ability to form large clusters. These results confirmed that phosphorylated CDCP1 promoted cancer progression mainly by forming large clusters as functional domains, which facilitated the recruitment and binding of cancer-related proteins and the transduction of downstream signaling pathways.

EGF promotes the accumulation of CDCP1 clusters in cancer cells

CDCP1 is considered to be an oncogene and is involved in tumorigenesis and progression.[31] Notably, cancer cells with high CDCP1 expression level are more capable of metastasis than those with low CDCP1 expression level.[26] This explains why CDCP1 expression is upregulated in most patients with cancer with poor prognosis.[5,32,33] The above data have shown that inhibition of CDCP1 activity significantly reduced the clustering ability. Therefore, we want to further investigate whether CDCP1 clusters change with upregulation of its expression and activation. Previous studies have shown that EGF can increase the migration ability of cancer cells[12] by increasing the expression level of CDCP1.[34] Thus, 100 ng/mL EGF was used to treat SK-MES-1 cells that were cultured in serum-free medium. After simulation with EGF at 37°C for 24 h, the formation of clusters on cell surfaces enhanced dramatically (Figures 7A–7D). The localization density of CDCP1 increased from 1952 ± 160 to 2800 ± 374 per μm^2 (Figure 7E). And SR-Tesseler analysis showed that the proportion of cluster area in EGF-treated group increased significantly from 2.59 ± 0.29% to 3.52 ± 0.54% (Figure 7G). However, there was no significant change in the number of clusters after EGF stimulation (control: 1.97 ± 0.24 per μm^2, +EGF: 1.96 ± 0.38 per μm^2) (Figure 7F). Furthermore, the percentage of large clusters containing localizations between 361 and 420 and larger than 481 increased significantly and that of small clusters (localizations <180) decreased markedly (Figure 7H). In addition, Western Blot analysis also confirmed that stimulation of EGF increased CDCP1 expression in cancer cells (Figures 7I and 7J).

Taken together, CDCP1 expression level and aggregation degree increased after stimulated by EGF. The increase of localization density and cluster area indicated that EGF promoted many smaller clusters and single proteins to converge and form larger and denser clusters. Based on these results, we reconfirmed that the large cluster was functional domain of CDCP1 that plays an important role in cancer cells, which could improve the efficiency of their interaction with various signaling molecules such as PKC and Src to activate downstream signals.

Conclusions

This work reveals the characteristic clustered distribution of CDCP1 in lung cancer and the mechanism by which its distribution is regulated by activity. We first analyzed the mRNA expression level of CDCP1 and its relationship with prognosis to determine the association between CDCP1 and NSCLC. We then used dSTORM to observe and quantitatively analyze the distribution of CDCP1 protein in NSCLC at different levels from cultured cell lines to extracted primary cells, and pathological tissue sections. All levels indicated that the expression of CDCP1 on the cell membrane of lung cancer was dramatically increased and aggregated into more, larger and denser clusters. This distribution pattern may function as an important domain which is conducive to its effect on promoting cell proliferation and metastasis in cancers.

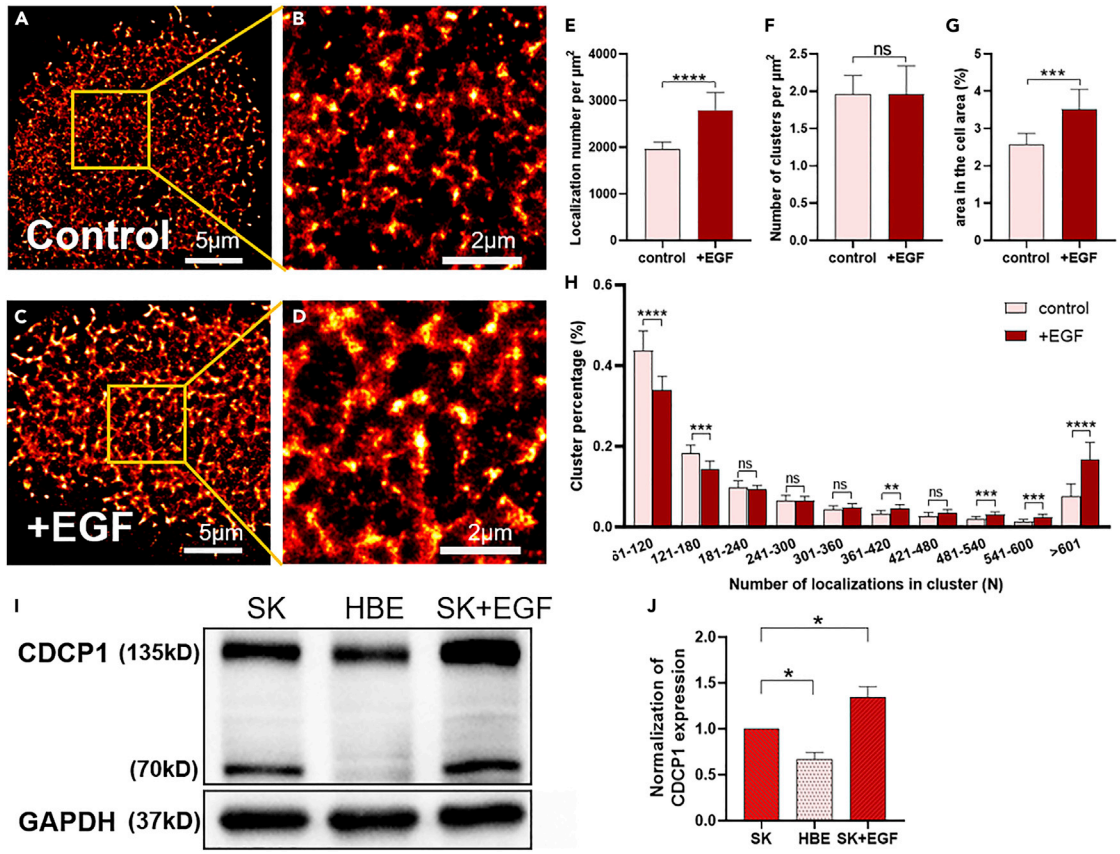

Figure 7. The changes of CDCP1 clusters after treatment of EGF and protein expression of CDCP1 by Western blot

(A–D) Reconstructed dSTORM images of CDCP1 on control (A) and EGF-treated (C) SK-MES-1 cell membranes, and the corresponding magnified images (B and D). (Scale bars: A and C, 5 μm; B and D, 2 μm).

(E) The number of CDCP1 localizations per μm^2 on control and EGF-treated SK-MES-1 cell membranes.

(F) The number of CDCP1 clusters per μm^2.

(G) The percentage of CDCP1 cluster area in each cell.

(H) The percentage of CDCP1 clusters containing different number of localizations. All data were obtained from 10 cell samples in 3 independent experiments (mean ± SD) and statistical significance was processed by two-tailed unpaired t-test.

(I) Western blot of CDCP1 in SK-MES-1 cells, HBE cells, and EGF-treated SK-MES-1 cells.

(J) Statistical analysis of CDCP1 expression levels. Data were obtained from three independent experiments (mean ± SD) and statistical significance was processed by two-tailed paired t-test. *$p < 0.05$, **$p < 0.01$, ***$p < 0.001$, ****$p < 0.0001$, and ns means not significant.

Also, we used PP2 and EGF to inhibit or promote the activity of CDCP1 protein, thereby observing how CDCP1 changes. The results indicated that the clustering ability of CDCP1, especially the ability to form large clusters, was significantly reduced when its function was inhibited, while the clustering characteristics were reversed when its function was promoted. This proved that the functional status of CDCP1 is directly related to its clustered distribution including the size and the density.

Moreover, we used dSTORM to observe the protein distribution in tissues, which considered the influence of complex factors such as the patients' microenvironment between tumor cells. The observation by super-resolution fluorescent microscope *in situ* provides us a deeper understanding of CDCP1 in lung cancer. We believe that super-resolution imaging of proteins in tissues will provide a new method for studying protein distribution and function in cancer and facilitate cancer diagnosis and target screening for targeted therapy.

Limitations of the study

In this study, we show the clustered distribution of CDCP1 in lung cancer and elucidate the mechanism of activity regulated distribution. Moreover, we used dSTORM to observe the protein distribution in tissues,

which considered the influence of complex factors such as the patients' microenvironment between tumor cells. However, it is unclear whether the histological grade of lung cancer is related to the distribution of CDCP1. Thus, additional studies are required for detailed correlation of the histological grade and clustering distribution of CDCP1.

STAR★METHODS

Detailed methods are provided in the online version of this paper and include the following:

- KEY RESOURCES TABLE
- RESOURCE AVAILABILITY
  - Lead contact
  - Materials availability
  - Data and code availability
- EXPERIMENTAL MODEL AND SUBJECT DETAILS
  - Culture of cell lines
  - Isolation of primary lung cells
- METHOD DETAILS
  - Cell sample preparation
  - Preparation of tissue section sample
  - dSTORM imaging
  - Data analysis
  - Western blot
  - CDCP1 gene expression analysis and Kaplan-Meier survival curve analysis
- QUANTIFICATION AND STATISTICAL ANALYSIS
  - Ethics approval
- ADDITIONAL RESOURCES

SUPPLEMENTAL INFORMATION

Supplemental information can be found online at https://doi.org/10.1016/j.isci.2023.106103.

ACKNOWLEDGMENTS

This work was financially supported by the Department of Finance of Jilin Province of China (No. 3D5204883429, 2020SCZT027, 3D5222865429), the National Natural Science Foundation of China (No. 2019SRCJ023, 22150003, 21727816 and 21721003), the Natural Science Foundation of Shandong Province (No. ZR2022QB218), the Scientific Instrument Developing Project of the Chinese Academy of Sciences (No. ZDKYYQ20220005). Graphical abstract was created with Bio-Render software, ©http://biorender.com.

AUTHOR CONTRIBUTIONS

Conceptualization, T.T. and J.G.; Methodology, Software, Writing - original draft preparation and editing, X.Q.; Writing – review & editing, T.T., J.G., and G.Z.; Data curation, Z.L.; Visualization, Investigation, J.Z.; Validation, Visualization, H.L., M.L., and B.L.; Project administration, Supervision, Y.F. and M.C.; Funding acquisition, Resources, H.W.

DECLARATION OF INTERESTS

The authors declare no competing interests.

INCLUSION AND DIVERSITY

We support inclusive, diverse, and equitable conduct of research.

Received: December 5, 2022
Revised: December 30, 2022
Accepted: January 27, 2023
Published: February 2, 2023

REFERENCES

1. Siegel, R.L., Miller, K.D., Fuchs, H.E., and Jemal, A. (2022). Cancer statistics, 2022. CA. Cancer J. Clin. *72*, 7–33. https://doi.org/10.3322/caac.21708.

2. Roller, J.F., Veeramachaneni, N.K., and Zhang, J. (2022). Exploring the evolving scope of neoadjuvant immunotherapy in NSCLC. Cancers *14*, 741. https://doi.org/10.3390/cancers14030741.

3. Zappa, C., and Mousa, S.A. (2016). Non-small cell lung cancer: current treatment and future advances. Transl. Lung Cancer Res. *5*, 288–300. https://doi.org/10.21037/tlcr.2016.06.07.

4. Hooper, J.D., Zijlstra, A., Aimes, R.T., Liang, H., Claassen, G.F., Tarin, D., Testa, J.E., and Quigley, J.P. (2003). Subtractive immunization using highly metastatic human tumor cells identifies SIMA135/CDCP1, a 135 kDa cell surface phosphorylated glycoprotein antigen. Oncogene *22*, 1783–1794. https://doi.org/10.1038/sj.onc.1206220.

5. Ikeda, J.i., Oda, T., Inoue, M., Uekita, T., Sakai, R., Okumura, M., Aozasa, K., and Morii, E. (2009). Expression of CUB domain containing protein (CDCP1) is correlated with prognosis and survival of patients with adenocarcinoma of lung. Cancer Sci. *100*, 429–433. https://doi.org/10.1111/j.1349-7006.2008.01066.x.

6. Nam, Y., Choi, C.M., Park, Y.S., Jung, H., Hwang, H.S., Lee, J.C., Lee, J.W., Lee, J.E., Kang, J.H., Jung, B.H., and Ji, W. (2022). CDCP1 expression is a potential biomarker of poor prognosis in resected stage I non-small-cell lung cancer. J. Clin. Med. *11*, 341. https://doi.org/10.3390/jcm11020341.

7. Wu, H., Shang, L.Q., Chen, R.L., Yang, S.M., Wang, S.L., Wang, J., and Sun, G. (2015). Significance of Trask protein interactions in brain metastatic cohorts of lung cancers. Tumour Biol. *36*, 4181–4187. https://doi.org/10.1007/s13277-015-3053-7.

8. Chiu, K.L., Kuo, T.T., Kuok, Q.Y., Lai, L.C., and Sher, Y.P. (2016). ADAM9 to enhance CDCP1 protein expression by suppressing miR-218 for lung tumor metastasis. J. Clin. Oncol. *34*, e23002. https://doi.org/10.1200/JCO.2016.34.15_suppl.e23002.

9. Martinko, A.J., Truillet, C., Julien, O., Diaz, J.E., Horlbeck, M.A., Whiteley, G., Blonder, J., Weissman, J.S., Bandyopadhyay, S., Evans, M.J., and Wells, J.A. (2018). Targeting RAS-driven human cancer cells with antibodies to upregulated and essential cell-surface proteins. Elife *7*, e31098. https://doi.org/10.7554/eLife.31098.

10. Wright, H.J., Arulmoli, J., Motazedi, M., Nelson, L.J., Heinemann, F.S., Flanagan, L.A., and Razorenova, O.V. (2016). CDCP1 cleavage is necessary for homodimerization-induced migration of triple-negative breast cancer. Oncogene *35*, 4762–4772. https://doi.org/10.1038/onc.2016.7.

11. Uekita, T., Fujii, S., Miyazawa, Y., Iwakawa, R., Narisawa-Saito, M., Nakashima, K., Tsuta, K., Tsuda, H., Kiyono, T., Yokota, J., and Sakai, R. (2014). Oncogenic Ras/ERK signaling activates CDCP1 to promote tumor invasion and metastasis. Mol. Cancer Res. *12*, 1449–1459. https://doi.org/10.1158/1541-7786.Mcr-13-0587.

12. Dong, Y., He, Y., de Boer, L., Stack, M.S., Lumley, J.W., Clements, J.A., and Hooper, J.D. (2012). The cell surface glycoprotein CUB domain-containing protein 1 (CDCP1) contributes to epidermal growth factor receptor-mediated cell migration. J. Biol. Chem. *287*, 9792–9803. https://doi.org/10.1074/jbc.M111.335448.

13. Casar, B., Rimann, I., Kato, H., Shattil, S.J., Quigley, J.P., and Deryugina, E.I. (2014). In vivo cleaved CDCP1 promotes early tumor dissemination via complexing with activated beta 1 integrin and induction of FAK/PI3K/Akt motility signaling. Oncogene *33*, 255–268. https://doi.org/10.1038/onc.2012.547.

14. Deryugina, E.I., Conn, E.M., Wortmann, A., Partridge, J.J., Kupriyanova, T.A., Ardi, V.C., Hooper, J.D., and Quigley, J.P. (2009). Functional role of cell surface CUB domain-containing protein 1 in tumor cell dissemination. Mol. Cancer Res. *7*, 1197–1211. https://doi.org/10.1158/1541-7786.MCR-09-0100.

15. Kryza, T., Khan, T., Puttick, S., Li, C., Sokolowski, K.A., Tse, B.W., Cuda, T., Lyons, N., Gough, M., Yin, J., et al. (2020). Effective targeting of intact and proteolysed CDCP1 for imaging and treatment of pancreatic ductal adenocarcinoma. Theranostics *10*, 4116–4133. https://doi.org/10.7150/thno.43589.

16. Harrington, B.S., He, Y., Davies, C.M., Wallace, S.J., Adams, M.N., Beaven, E.A., Roche, D.K., Kennedy, C., Chetty, N.P., Crandon, A.J., et al. (2016). Cell line and patient-derived xenograft models reveal elevated CDCP1 as a target in high-grade serous ovarian cancer. Br. J. Cancer *114*, 417–426. https://doi.org/10.1038/bjc.2015.471.

17. He, Y., Wu, A.C., Harrington, B.S., Davies, C.M., Wallace, S.J., Adams, M.N., Palmer, J.S., Roche, D.K., Hollier, B.G., Westbrook, T.F., et al. (2016). Elevated CDCP1 predicts poor patient outcome and mediates ovarian clear cell carcinoma by promoting tumor spheroid formation, cell migration and chemoresistance. Oncogene *35*, 468–478. https://doi.org/10.1038/onc.2015.101.

18. Lim, S.A., Zhou, J., Martinko, A.J., Wang, Y.H., Filippova, E.V., Steri, V., Wang, D., Remesh, S.G., Liu, J., Hann, B., et al. (2022). Targeting a proteolytic neoepitope on CUB domain containing protein 1 (CDCP1) for RAS-driven cancers. J. Clin. Invest. *132*, e154604. https://doi.org/10.1172/JCI154604.

19. Gao, J., Wang, Y., Cai, M., Pan, Y., Xu, H., Jiang, J., Ji, H., and Wang, H. (2015). Mechanistic insights into EGFR membrane clustering revealed by super-resolution imaging. Nanoscale *7*, 2511–2519. https://doi.org/10.1039/c4nr04962d.

20. Zhao, G., Li, H., Gao, J., Cai, M., Xu, H., Shi, Y., Wang, H., and Wang, H. (2021). Insight into the different channel proteins of human red blood cell membranes revealed by combined dSTORM and AFM techniques. Anal. Chem. *93*, 14113–14120. https://doi.org/10.1021/acs.analchem.1c02382.

21. Levet, F., Hosy, E., Kechkar, A., Butler, C., Beghin, A., Choquet, D., and Sibarita, J.B. (2015). SR-Tesseler: a method to segment and quantify localization-based super-resolution microscopy data. Nat. Methods *12*, 1065–1071. https://doi.org/10.1038/nmeth.3579.

22. Li, H., Zhang, J., Shi, Y., Zhao, G., Xu, H., Cai, M., Gao, J., and Wang, H. (2022). Mechanism of INSR clustering with insulin activation and resistance revealed by super-resolution imaging. Nanoscale *14*, 7747–7755. https://doi.org/10.1039/d2nr01051h.

23. Law, M.E., Ferreira, R.B., Davis, B.J., Higgins, P.J., Kim, J.S., Castellano, R.K., Chen, S., Luesch, H., and Law, B.K. (2016). CUB domain-containing protein 1 and the epidermal growth factor receptor cooperate to induce cell detachment. Breast Cancer Res. *18*, 80. https://doi.org/10.1186/s13058-016-0741-1.

24. Alajati, A., Guccini, I., Pinton, S., Garcia-Escudero, R., Bernasocchi, T., Sarti, M., Montani, E., Rinaldi, A., Montemurro, F., Catapano, C., et al. (2015). Interaction of CDCP1 with HER2 enhances HER2-driven tumorigenesis and promotes trastuzumab resistance in breast cancer. Cell Rep. *11*, 564–576. https://doi.org/10.1016/j.celrep.2015.03.044.

25. Spassov, D.S., Baehner, F.L., Wong, C.H., McDonough, S., and Moasser, M.M. (2009). The transmembrane src substrate trask is an epithelial protein that signals during anchorage deprivation. Am. J. Pathol. *174*, 1756–1765. https://doi.org/10.2353/ajpath.2009.080890.

26. Liu, H., Ong, S.E., Badu-Nkansah, K., Schindler, J., White, F.M., and Hynes, R.O. (2011). CUB-domain-containing protein 1 (CDCP1) activates Src to promote melanoma metastasis. Proc. Natl. Acad. Sci. USA *108*, 1379–1384. https://doi.org/10.1073/pnas.1017228108.

27. Bhatt, A.S., Erdjument-Bromage, H., Tempst, P., Craik, C.S., and Moasser, M.M. (2005). Adhesion signaling by a novel mitotic substrate of src kinases. Oncogene *24*, 5333–5343. https://doi.org/10.1038/sj.onc.1208582.

28. Chen, Y., Harrington, B.S., Lau, K.C.N., Burke, L.J., He, Y., Iconomou, M., Palmer, J.S., Meade, B., Lumley, J.W., and Hooper, J.D. (2017). Development of an enzyme-linked immunosorbent assay for detection of CDCP1 shed from the cell surface and present in colorectal cancer serum specimens. J. Pharm. Biomed. Anal. *139*, 65–72. https://doi.org/10.1016/j.jpba.2017.02.047.

29. Uekita, T., Jia, L., Narisawa-Saito, M., Yokota, J., Kiyono, T., and Sakai, R. (2007). CUB domain-containing protein 1 is a novel regulator of anoikis resistance in lung adenocarcinoma. Mol. Cell Biol. *27*, 7649–7660. https://doi.org/10.1128/Mcb.01246-07.

30. Kajiwara, K., Chen, P.K., Abe, Y., Okuda, S., Kon, S., Adachi, J., Tomonaga, T., Fujita, Y., and Okada, M. (2022). Src activation in lipid rafts confers epithelial cells with invasive potential to escape from apical extrusion during cell competition. Curr. Biol. *32*, 3460–3476.e6. https://doi.org/10.1016/j.cub.2022.06.038.

31. Khan, T., Kryza, T., Lyons, N.J., He, Y., and Hooper, J.D. (2021). The CDCP1 signaling hub: a target for cancer detection and therapeutic intervention. Cancer Res. *81*, 2259–2269. https://doi.org/10.1158/0008-5472.Can-20-2978.

32. Turdo, F., Bianchi, F., Gasparini, P., Sandri, M., Sasso, M., De Cecco, L., Forte, L., Casalini, P., Aiello, P., Sfondrini, L., et al. (2016). CDCP1 is a novel marker of the most aggressive human triple-negative breast cancers. Oncotarget *7*, 69649–69665. https://doi.org/10.18632/oncotarget.11935.

33. Miyazawa, Y., Uekita, T., Hiraoka, N., Fujii, S., Kosuge, T., Kanai, Y., Nojima, Y., and Sakai, R. (2010). CUB domain-containing protein 1, a prognostic factor for human pancreatic cancers, promotes cell migration and extracellular matrix degradation. Cancer Res. *70*, 5136–5146. https://doi.org/10.1158/0008-5472.CAN-10-0220.

34. Adams, M.N., Harrington, B.S., He, Y., Davies, C.M., Wallace, S.J., Chetty, N.P., Crandon, A.J., Oliveira, N.B., Shannon, C.M., Coward, J.I., et al. (2015). EGF inhibits constitutive internalization and palmitoylation-dependent degradation of membrane-spanning procancer CDCP1 promoting its availability on the cell surface. Oncogene *34*, 1375–1383. https://doi.org/10.1038/onc.2014.88.

35. Fu, Y., Jing, Y., Gao, J., Li, Z., Wang, H., Cai, M., and Tong, T. (2020). Variation of Trop2 on non-small-cell lung cancer and normal cell membranes revealed by super-resolution fluorescence imaging. Talanta *207*, 120312. https://doi.org/10.1016/j.talanta.2019.120312.

36. Zheng, C., Sun, Y.H., Ye, X.L., Chen, H.Q., and Ji, H.B. (2011). Establishment and characterization of primary lung cancer cell lines from Chinese population. Acta Pharmacol. Sin. *32*, 385–392. https://doi.org/10.1038/aps.2010.214.

37. Choi, S.J., Lee, H., Choe, C., Shin, Y.S., Lee, J., Moon, S.H., and Kim, J. (2014). Establishment and characterization of a lung cancer cell line, SMC-L001, from a lung adenocarcinoma. In Vitro Cell. Dev. Biol. Anim. *50*, 519–526. https://doi.org/10.1007/s11626-014-9736-3.

38. Ovesný, M., Křížek, P., Borkovec, J., Svindrych, Z., and Hagen, G.M. (2014). ThunderSTORM: a comprehensive ImageJ plug-in for PALM and STORM data analysis and super-resolution imaging. Bioinformatics *30*, 2389–2390. https://doi.org/10.1093/bioinformatics/btu202.

39. Tang, Z., Kang, B., Li, C., Chen, T., and Zhang, Z. (2019). GEPIA2: an enhanced web server for large-scale expression profiling and interactive analysis. Nucleic Acids Res. *47*, W556–W560. https://doi.org/10.1093/nar/gkz430.

40. Nagy, Á., Munkácsy, G., and Győrffy, B. (2021). Pancancer survival analysis of cancer hallmark genes. Sci. Rep. *11*, 6047. https://doi.org/10.1038/s41598-021-84787-5.

STAR★METHODS

KEY RESOURCES TABLE

REAGENT or RESOURCE	SOURCE	IDENTIFIER
Antibodies		
Rabbit monoclonal anti-CDCP1	Abcam	Cat#ab245839
Alexa Fluor 647-conjugated goat anti-rabbit IgG	Invitrogen	Cat#A-21245, RRID: AB_2535813
Rabbit polyclonal anti-CDCP1	Cell Signaling Technology	Cat#4115S, RRID: AB_2078818
Mouse monoclonal anti-GAPDH	Beyotime	Cat#AF0006, RRID: AB_2715590
goat anti-rabbit secondary antibody	Beyotime	Cat#A0208, RRID: AB_2892644
goat anti-mouse IgG secondary antibody	Beyotime	Cat#A0216, RRID: AB_2860575
Biological samples		
Lung cancer patient's lung cancer tissue	The Second Hospital of Jilin University	N/A
Chemicals, peptides, and recombinant proteins		
Animal-Free Recombinant Human EGF	PeperoTech	Cat#AF-100-15
PP2	Aladdin	Cat#172889-27-9
Collagenase III	Sangon Biotech	Cat#A004206
β-mercaptoethanol	Sigma-Aldrich	Lot#SHBF1470V
Glucose oxidase	Sigma-Aldrich	Lot#BCBP8730V
Catalase	Sigma-Aldrich	Lot#SLBG8704V
Agar	DING GUO	Cat#B047102400
RIPA Lysis Buffer	Beyotime	Cat#P0013
Protease inhibitors (PMSF)	Beyotime	Cat#ST506
SDS-PAGE gel	New Cell & Molecular Biotech Co. Ltd	Cat#PN202
PVDF membranes	Immobilon®-P	Lot#R1NB68665
Blocking buffer	Genefist	Cat#GF1815
TBST	Sangon Biotech	Cat#C520009-0500
High-sig ECL solution	Tanon	Cat#180-501
MEM medium	Biological Industries	Lot#8121528
RPMI-1640 medium	Biological Industries	Lot#8122651
Fetal bovine serum	Gibco	Lot#2414839RP
TetraSpeck microspheres	Invitrogen	Lot#2155302
Hoechst 33342	Beyotime	Cat#C1022
Critical commercial assays		
BCA protein kit	Thermo	Lot#TK274307
Deposited data		
Original western blot images	This paper	see Figure S2
Experimental models: Cell lines		
Human: HBE	Shanghai Institute of Biological Sciences	Fu et al.[35]
Human: SK-MES-1	Shanghai Institute of Biological Sciences	TCHu110
Software and algorithms		
GraphPad Prism8	GraphPad	https://www.graphpad.com/
ImageJ	ImageJ	https://imagej.nih.gov/ij/
SR-Tesseler	Levet et al.[21]	https://doi.org/10.1038/nmeth.3579
Gepia2 database	GEPIA	http://gepia2.cancer-pku.cn, version 2
Kaplan-Meier plotter	Kaplan-Meier plotter	http://kmplot.com/analysis/

RESOURCE AVAILABILITY

Lead contact

Further information and requests for resources should be directed to and will be fulfilled by the lead contact, Ti Tong (tongti@jlu.edu.cn).

Materials availability

This study did not generate new unique reagents.

Data and code availability

This paper did not report any original code; The raw data of Western Blot was shown in Figure S2; Any additional information required to reanalyze the data reported in this paper is available from the lead contact upon request.

EXPERIMENTAL MODEL AND SUBJECT DETAILS

Culture of cell lines

The normal human bronchial epithelial cell lines (HBE) and human lung cancer cell lines (SK-MES-1) were purchased from the Shanghai Institute of Biological Sciences (Shanghai, China).

HBE cells were cultured in RPMI-1640 medium (Biological Industries, BI). SK-MES-1 cells were cultured in MEM medium (Biological Industries, BI). They were maintained in suitable medium containing 10% fetal bovine serum (FBS, Gibco) and penicillin-streptomycin (BI) in a humidified environment with 5% CO2 at 37°C.

Before dSTORM imaging, they were divided into a dish where a clean coverslip (22 mm × 22 mm, Fisher) was placed and cultured at least 24h. Samples can be prepared when the cells reached a confluence of 50%–70%. For EGF (100 μg/mL in PBS; PeperoTech) treatment, cells grown in serum-free media for 24h were incubated in media containing 100ng/mL EGF for 24h. As for PP2 (2 mM in DMSO; Aladdin) treatment, they were incubated in media containing 2 μM PP2 for 24h prior to sample preparation.

Isolation of primary lung cells

The study was approved by the Ethics Review Committee of the Second Hospital of Jilin University. Informed consent was obtained from each patient. Lung cancer tissues and paired normal tissues were freshly isolated from 3 patients who underwent surgery at the Second Hospital of Jilin University. They were NSCLC patients who had undergone surgical treatment, and all tissue specimens were verified by pathological examination. The clinicopathological characteristics of the 3 patients, including sex, age, smoking history, histology, and tumor-lymph node-metastasis (TNM) stages were summarized in Table S2. All the clinical samples were washed with PBS five times and necrotic tissue was removed. We divided each piece of tissue into two parts, one for growing primary cells and the other for making tissue slices. The piece of tissue that prepared for growing primary cells was cut up with surgical scissors in the ACL4 medium.[36,37] For tumor fragment, we used a 1 mL pipette tip to blow over 50 times until it dispersed into individual cancer cells. For normal tissue fragment, we treated it with collagenase III (1 mg/mL; Sangon Biotech) for 2h by shaking at 37°C. And then, the supernatant was separated by centrifugation (1000rpm, 4min) after adding the same amount of FBS.[35] After that, we used a 60-80 μm^2 filter to remove the remaining small pieces from RPMI-1640 medium resuspension. Finally, they were cultured in the dish containing RPMI-1640 medium with 20% FBS, streptomycin-penicillin in a 5% CO2 atmosphere at 37°C for 4 days.

METHOD DETAILS

Cell sample preparation

For cell samples, the culture medium was discarded, and the samples were washed with PBS three times. And then, they were fixed with 4% paraformaldehyde (PFA) in the dark for 30 min at room temperature to immobilize the plasma membrane molecules. After washing with PBS three times, the samples were blocked by incubating with 3% (BSA, m/v) for 30min. CDCP1 antibody (Abcam, ab245839) was diluted 100 times with 3% BSA, and the samples were incubated with the antibody at 4°C overnight. Next, the cells were washed with PBS three times and stained with Alexa Fluor 647-conjugated goat anti-rabbit IgG (2 μg/mL in 3% BSA; Invitrogen, A21245) for 30min in the dark. Finally, the samples were washed with

PBS three times to remove excess fluorescent dye. Before sealing the sample with nail polish, 100 μL of imaging buffer containing Tris (50 mM, pH 8.0), NaCl (10 mM), glucose (10% w/v), glucose oxidase (500 μg/mL; Sigma), catalase (40 μg/mL; Sigma), and β-mercaptoethanol (β-ME; 1% v/v; Sigma) was dropped onto a large slide (24 mm × 50 mm), and the small slide containing the seeded cells was covered on the large slide.

Preparation of tissue section sample

We first cut the tissues into about 0.5 × 0.5 × 0.5 cm^3 pieces and soaked them in 4% PFA for 7h. Then, it was embedded in agar (DING GUO, B047102400) and sliced into 30 μm slices with a vibratome (ZQP-86, Zhixin Instrument Co., Ltd, Shanghai, China). After rinsing with PBS five times, the sample was incubated in 3% BSA for 1h and then incubated overnight with primary antibody (1:50 dilution; Abcam, ab245839) at 4°C. Next, the sample was washed three times and stained with Alexa Fluor 647-conjugated goat anti-rabbit IgG (2 μg/mL in 3% BSA; Invitrogen, A21245) for 1h in the dark. For nuclear staining, we used Hoechst 33342 (Beyotime, C1022) to stain the sections for 5 min. Finally, we applied the above method to seal the sample.

dSTORM imaging

We used a Nikon Ti-E inverted fluorescence microscope with a 100× TIRF lens (numerical aperture 1.49; Nikon, Japan). During the imaging process, a 640 nm laser was used for fluorescent excitation of Alexa647, and a low-power 405 nm laser (0.5 mW) was used to increase the number of on-state fluorophores. The equipment also included an excitation filter (ZT405/488/532/647x, Chroma), a dichromic mirror, an emission filter, and an electron-multiplying CCD camera (Andor Ixon Ultra 888) for imaging. Micro-Manager software was used to continuously capture 5000 images for each cell (or tissue section) with a 25 ms exposure time. During the image collection, the *x*-*y* drift was corrected using 100 nm TetraSpeck microspheres (Invitrogen) and the *z*-drift was eliminated using Perfect Focus System provided by Nikon microscopy.

Data analysis

We used the ThunderSTORM,[38] a plugin in ImageJ, to process the raw data. Figure S3A showed the parameter settings for data reconstruction, and Figures S3B and S3C showed the TIRF images and the reconstructed dSTORM images. Here, we use the tool to circle the cell and calculate its area by ImageJ.

SR-Tesseler was used to analyze cluster data for CDCP1 in each cell[21] and its "ROI" tool was used to select the cell membrane to be analyzed. First, bisectors were drawn between the two nearest localizations, and the ROI was divided into numerous polygons based on the localization density (see Figures S4A, S4B, S4E, and S4F). The localization density of a polygon was defined as δ_i^1 and the average localization density of ROI was defined as δ. Then we selected the polygons whose localization density δ_i^1 were greater than δ, and defined the region combined by adjacent polygons as an object (see Figures S4C and S4G). The localization density within an object was defined as δ_i^0 and the average localization density within all objects was defined as δ^0. And finally, the objects with higher localization density δ_i^0 than the average localization density δ^0 were selected as clusters (see Figures S4D and S4H). With this method, the detailed information of clusters could be extracted for further statistical analysis.

For the data of tissue sections, we first used ImageJ to circle the cell membrane regions of individual cells and measured the area. The corresponding data of individual cells were extracted by ImageJ, and then analyzed according to the above method.

Western blot

Cells were treated with RIPA Lysis Buffer (Beyotime, #P0013) containing protease inhibitors (Beyotime, ST506) and the concentrations of total protein were quantified by a BCA protein kit (Thermo, TK274307). Lysed protein was separated by 10% SDS-PAGE gel (New Cell & Molecular Biotech Co. Ltd) and transferred onto PVDF membranes (Immobilon-P). The membranes were blocked with blocking buffer (Genefist, CAT#.GF1815) for 30 min and then were incubated with primary antibodies at 4°C overnight. The primary antibodies included anti-CDCP1 (1:1000; CST,4115S), anti-GAPDH (1:2000; Beyotime, AF0006). After washing with TBST (Sangon Biotech), the appropriate HRP-conjugated secondary antibodies (1:5000; Beyotime, A0216 for goat-*anti*-mouse and A0208 for goat-*anti*-rabbit) were used to incubate the membranes for 1 h. Finally, the membranes were washed again and the signals were visualized by High-sig ECL solution

(Tanon, No.180-501) using Tanon Imaging System. ImageJ was used to measure and analyze the results of the Western Blot.

CDCP1 gene expression analysis and Kaplan-Meier survival curve analysis

The mRNA levels of CDCP1 in pan-cancer including LUAD and LUSC were identified from the Gepia2 database (GEPIA, http://gepia2.cancer-pku.cn, version 2) and the RNA sequencing data of 9736 tumors and 8587 normal samples were from the TCGA and the GTEx projects.[39]

We used the Kaplan-Meier plotter (http://kmplot.com/analysis/) to analyze the relationship of CDCP1 gene expression with OS and RFS in LUAD and LUSC based on the hazard ratios (HR) and log-rank p-values.[40]

QUANTIFICATION AND STATISTICAL ANALYSIS

Statistical analyses were performed using Prism software (GraphPad Prism software version 8.0.2). Differences between groups were analyzed by Student's t test (data of dSTORM imagign) or one-way ANOVA followed by Dunnett's t test (data of western blot). The results of quantitative data in histograms were presented as mean $\pm$ SD and the data were considered significant when $p < 0.05$. The meaning of asterisks number were *$p < 0.05$, **$p < 0.01$, ***$p < 0.001$, ****$p < 0.0001$, and ns means not significant.

Ethics approval

The study was approved by the Ethics Review Committee of the Second Hospital of Jilin University (Permit protocol: 2020-069) and informed consent was obtained from each patient.

ADDITIONAL RESOURCES

This paper did not create any additional resources.